

Semiclassical Coulomb-scattering model for strong-field tunneling ionization

Qing Zhao(赵晴), Yigen Peng(彭易根), Jiayin Che(车佳殷), Chao Chen(陈超), Shang Wang(王赏), Guoguo Xin(辛国国), and Yanjun Chen(陈彦军)

Citation: Chin. Phys. B, 2025, 34 (**9**): 093201. DOI: 10.1088/1674-1056/ade06e
http://cpb.iphy.ac.cn; http://iopscience.iop.org/cpb

What follows is a list of articles you may be interested in

Attosecond ionization time delays in strong-field physics

Yongzhe Ma(马永哲), Hongcheng Ni(倪宏程), and Jian Wu(吴健)
Chin. Phys. B, 2024, 33 (**1**): 013201. DOI: 10.1088/1674-1056/ad0e5d

Taking snapshots of a moving electron wave packet in molecules using photoelectron holography in strong-field tunneling ionization

Mingrui He(何明睿), Yang Fan(樊洋), Yueming Zhou(周月明), and Peixiang Lu(陆培祥)
Chin. Phys. B, 2021, 30 (**12**): 123202. DOI: 10.1088/1674-1056/abf7a7

Imprint of transient electron localization in H_2^+ using circularly-polarized laser pulse

Jianghua Luo(罗江华), Jun Li(李军), and Huafeng Zhang(张华峰)
Chin. Phys. B, 2020, 29 (**12**): 123201. DOI: 10.1088/1674-1056/abbbe1

Above-threshold ionization of hydrogen atom in chirped laser fields

Yuan-Yuan Ni(倪园园), Song-Feng Zhao(赵松峰), Xiao-Yong Li(李小勇), Guo-Li Wang(王国利), Xiao-Xin Zhou(周效信)
Chin. Phys. B, 2018, 27 (**7**): 073203. DOI: 10.1088/1674-1056/27/7/073203

Photoelectron angular distributions of H ionization in low energy regime: Comparison between different potentials

Shu-Na Song(宋舒娜), Hao Liang(梁昊), Liang-You Peng(彭良友), Hong-Bing Jiang(蒋红兵)
Chin. Phys. B, 2016, 25 (**9**): 093201. DOI: 10.1088/1674-1056/25/9/093201

SPECIAL TOPIC — Ultrafast physics in atomic, molecular and optical systems

Semiclassical Coulomb-scattering model for strong-field tunneling ionization

Qing Zhao(赵晴)[1,2,†], Yigen Peng(彭易根)[2,†], Jiayin Che(车佳殷)[2,3], Chao Chen(陈超)[2,4], Shang Wang(王赏)[1,‡], Guoguo Xin(辛国国)[5,§], and Yanjun Chen(陈彦军)[2,¶]

[1] *College of Physics and Hebei Key Laboratory of Photophysics Research and Application, Hebei Normal University, Shijiazhuang* 050010, *China*

[2] *College of Physics and Information Technology and Quantum Materials and Devices Key Laboratory of Shaanxi Province's High Education Institution, Shaan'xi Normal University, Xi'an* 710119, *China*

[3] *School of Physics, Henan Normal University, Xinxiang* 453007, *China*

[4] *College of Physics and Electronic Engineering, Xingtai University, Xingtai* 054001, *China*

[5] *School of Physics, Northwest University, Xi'an* 710127, *China*

(Received 2 April 2025; revised manuscript received 20 May 2025; accepted manuscript online 4 June 2025)

This study analytically examines the ionization of atoms in strong near-circular laser fields. The classic Keldysh–Rutherford (KR) Coulomb-scattering (CS) model [*Phys. Rev. Lett.* **121** 123201 (2018)] successfully explained the attoclock experimental curve for the H atom at lower laser intensities. Here, we develop a semiclassical model that includes the initial conditions related to the quantum properties of tunneling in the KR model at the beginning of the scattering process. This model is able to explain recent attoclock experimental curves over a wider range of laser and atomic parameters. Our results show the importance of system symmetry and quantum effects in attoclock measurements, suggesting the complex role of the Coulomb potential in strong-field ionization.

Keywords: tunneling ionization, Coulomb scattering, attoclock

PACS: 32.80.–t, 42.65.Re, 42.50.Hz

DOI: 10.1088/1674-1056/ade06e **CSTR:** 32038.14.CPB.ade06e

1. Introduction

When atoms are exposed to a strong near-infrared laser field, the valence electron can be ionized through tunneling.[1] The tunneling ionization process can be described by the strong-field approximation (SFA),[2] where the Coulomb potential is neglected. For strong elliptically polarized laser fields with high ellipticity, the atomic photoelectron momentum distribution (PMD) is ring-like. Compared with SFA predictions, the ring-like distribution measured in actual experiments presents a small rotation characterized by the offset angle θ. This angle is caused by the Coulomb effect and depends on laser and atomic parameters. In recent years, experimental techniques have been developed to use this angle to detect the attosecond tunneling dynamics of electrons. The related technique has been called attosecond angle streaking or attoclock,[3–6] which has aroused great research interest.[7–11] Many attoclock experiments have been performed to probe the tunneling time (i.e., the time spent by an electron under the barrier during the process of tunneling). While some experiments show that tunneling requires a finite time,[12–14] others show that tunneling is instantaneous.[15–18]

To obtain time information from the measured offset angle, one needs to establish a clear mapping between the corresponding time and this angle.[19] To do so, one first needs to develop a time-dependent analytical model that includes the Coulomb potential to describe the ionization dynamics of atoms in a strong laser field. This mapping can then be deduced from the developed model. In recent years, some strong-field models that include the Coulomb potential have been established,[20,21] such as the trajectory-based Coulomb-SFA (TC-SFA) model,[22] the analytical R-matrix (ARM) theory,[18] the Keldysh–Rutherford (KR) model,[23] and the extended KR model.[24] The TC-SFA considers the Coulomb effect after tunneling and describes it through the numerical solution of the Newton equation. The ARM considers the Coulomb effect under the potential barrier and describes it by incorporating the Coulomb potential into the saddle-point equation. The KR considers the Coulomb effect after tunneling and describes it using classical Coulomb scattering theory. The extended KR is somewhat similar to the TC-SFA model but solves the Newton equation analytically. Due to the complexity of the analytical treatment of the Coulomb interaction

[†]The authors contributed equally to this paper.

[‡]Corresponding author. E-mail: phywangshang@163.com

[§]Corresponding author. E-mail: xinguo@nwu.edu.cn

[¶]Corresponding author. E-mail: chenyjhb@gmail.com

© 2025 Chinese Physical Society and IOP Publishing Ltd. All rights, including for text and data mining, AI training, and similar technologies, are reserved.

in strong-field ionization, different approximations have been applied in these models. As a result, the predictions of these models for the offset angle and the corresponding time deduced from this angle differ somewhat from each other. In contrast to other models, the KR model is able to reproduce the experimental curve of the H atom offset angle at low laser intensities and provides a simple and intuitive physical picture that explains the origin of the offset angle.

Very recently, a semiclassical strong-field model known as the tunneling-response-classical-motion (TRCM) model[25–28] has also been developed to explain the origin of the offset angle in attoclock. This model attributes the complex Coulomb effect to an initial velocity at the tunnel exit from the perspective of the symmetry of the system. In this respect, it is somewhat similar to the KR scattering model, but it also considers the initial conditions at the tunnel exit given by the SFA[22,29,30] using saddle-point theory.[1] It is interesting to consider what would happen if the SFA initial conditions were also introduced into the KR model, as the TRCM can quantitatively reproduce some recent attoclock experimental curves and provides a consistent explanation for the results obtained in experiments.

In this paper, we develop a semiclassical CS model by incorporating the SFA initial conditions into the general KR model. The developed semiclassical model, called CS-SFA, not only explains a series of recent attoclock experiments using a wider range of laser and atomic parameters but also provides an intuitive physical picture for the origin of the offset angle. Our results show that when the electron exits the laser-Coulomb-formed barrier through tunneling, it has an initial velocity at the tunnel exit that reflects the quantum nature of tunneling and is determined by the saddle-point equation for the SFA. The electron is then classically elastically scattered by the Coulomb potential with central symmetry. This scattering results in a momentum shift. This shift, along with the initial velocity at the tunnel exit, quantifies the scattering angle, which is equal to the offset angle in attoclock.

2. Coulomb-scattering SFA

In this section, we introduce the Coulomb-inclusive model developed in this paper to describe the strong-field ionization of atoms.

2.1. SFA

We begin our discussions with the SFA.[31–33] According to the SFA, the tunneling mechanism dominates in strong-field ionization. In the length gauge, the SFA amplitude of a photoelectron with drift momentum $\boldsymbol{p}$ can be written as[2]

$$c(\boldsymbol{p}) = -\mathrm{i}\int_0^{T_\mathrm{p}} \mathrm{d}t'\, \boldsymbol{E}(t')\cdot \boldsymbol{d}_i[\boldsymbol{p}+\boldsymbol{A}(t')]\,\mathrm{e}^{\mathrm{i}S(\boldsymbol{p},t')}. \tag{1}$$

Here, the term $S(\boldsymbol{p},t') = \int^{t'}\{[\boldsymbol{p}+\boldsymbol{A}(t'')]^2/2 + I_\mathrm{p}\}\,\mathrm{d}t''$ is the semiclassical action, and T_p is the length of the total pulse. The term $\boldsymbol{d}_i(\boldsymbol{v}) = \langle \boldsymbol{v}|\boldsymbol{r}|0\rangle$ is the transition matrix element between the ground state $|0\rangle$ and the continuum state $|\boldsymbol{v}\rangle$, and $\boldsymbol{A}(t)$ is the vector potential of the electric field $\boldsymbol{E}(t)$. The temporal integral in the expression of $c(\boldsymbol{p})$ can be evaluated using the saddle-point method,[1,2] by solving the following equation:

$$[\boldsymbol{p}+\boldsymbol{A}(t_\mathrm{s})]^2/2 = -I_\mathrm{p}. \tag{2}$$

The solution $t_\mathrm{s} = t_0 + \mathrm{i}t_x$ of the above equation is complex; however, the real part t_0 can be understood as the tunneling-out time at which the tunneling electron exits the barrier. If we do not consider the Coulomb potential, the tunneling-out time t_0 also equals the ionization time at which the electron is free.

From a semiclassical view of point, at time t_0, the exit position $\boldsymbol{r}_0$ (i.e., the initial position at t_0) of the tunneling electron can be evaluated using $\boldsymbol{r}_0 \equiv \boldsymbol{r}(t_0) = \mathrm{Re}(\int_{t_0+\mathrm{i}t_x}^{t_0}[\boldsymbol{p}+\boldsymbol{A}(t')]\,\mathrm{d}t')$, and the exit velocity $\boldsymbol{v}(t_0)$ (i.e., the initial velocity at t_0) can be evaluated using $\boldsymbol{v}(t_0) = \boldsymbol{p}+\boldsymbol{A}(t_0)$. Note that, according to Eq. (2), the exit velocity $\boldsymbol{v}(t_0)$ also agrees with the relation $\boldsymbol{v}(t_0) \approx -\mathrm{Re}[\boldsymbol{A}(t_\mathrm{s})] + \boldsymbol{A}(t_0)$. This reflects the basic quantum effect of the system in tunneling, characterized by the complex time t_s. This velocity expression also gives the mapping between the drift momentum $\boldsymbol{p}$ and the ionization time t_0 in the SFA, namely,

$$\boldsymbol{p} \equiv \boldsymbol{p}(t_0) = \boldsymbol{v}(t_0) - \boldsymbol{A}(t_0). \tag{3}$$

2.2. CS-SFA

Next, we develop a semiclassical CS SFA (CS-SFA) model by introducing the initial conditions given by the quantum model of SFA into the classical CS model, i.e., the KR model. At the tunnel exit ($r_0 \sim 10$ a.u. for the laser and atomic parameters commonly used in experiments), the electron is not far from the nucleus, and it is also significantly influenced by the Coulomb force $\boldsymbol{F}_\mathrm{c} = -\frac{Z}{r_0^3}\boldsymbol{r}_0$. Here, Z is the nuclear charge and $r_0 = |\boldsymbol{r}_0|$.

2.2.1. Coulomb scattering

Based on the physical picture given by the KR model, we assume that when the electron exits the barrier at t_0 with the exit position $\boldsymbol{r}(t_0)$ and the exit velocity $\boldsymbol{v}(t_0)$, it is immediately scattered by the Coulomb potential. During the scattering process, the electron momentum changes from $\boldsymbol{p}$ to $\boldsymbol{p}'$. The momentum $\boldsymbol{p}'$ of the scattered electron is given by the following equation:

$$\boldsymbol{p}' = \boldsymbol{p} + \boldsymbol{v}_i = \boldsymbol{v}(t_0) + \boldsymbol{v}_i - \boldsymbol{A}(t_0). \tag{4}$$

Here, $|\boldsymbol{v}_i| = |\Delta\boldsymbol{p}| = |\boldsymbol{p}'-\boldsymbol{p}|$ is the momentum shift induced by the Coulomb scattering and can be determined using the

classical Coulomb scattering formula with the assumption of elastic scattering from $\boldsymbol{p}$ to $\boldsymbol{p}'$. That is,[23,24]

$$|\Delta\boldsymbol{p}| = 2|\boldsymbol{p}|\sin\left(\frac{\theta'}{2}\right) = \frac{2Z}{pr_\mathrm{b}} \tag{5}$$

with $p = |\boldsymbol{p}| \approx |\boldsymbol{p}'|$, $\sin(\frac{\theta'}{2}) = Z/(p^2 r_\mathrm{b})$ and $r_\mathrm{b} \approx r_0$. Here, θ' is the scattering angle, and the tunnel exit r_0 can be approximately expressed as $r_0 \approx I_\mathrm{p}/|\boldsymbol{E}(t_0)|$. The elastic-scattering assumption is applicable for the condition $|V(r_0)| = Z/r_0 \ll \boldsymbol{p}^2/2 = [\boldsymbol{v}(t_0) - \boldsymbol{A}(t_0)]^2/2$. Our simulations based on saddle-point theory show that the value of the initial velocity $|\boldsymbol{v}(t_0)|$ is small only when the Keldysh parameter[31] $\gamma = \omega\sqrt{2I_\mathrm{p}(1+\epsilon^2)}/E_\mathrm{L}$ is small enough. Here, the term E_L represents the maximal laser amplitude relative to the peak intensity I, ϵ is the laser ellipticity, and ω is the laser frequency.

2.2.2. Offset angle formula

The offset angle θ is related to the electron that exits the barrier at the peak time of the laser field and therefore has the maximal amplitude. According to our CS presumption, in this case, the scattering angle θ' of the electron equals the offset angle θ. We assume that the laser field $\boldsymbol{E}(t)$ has the form $\boldsymbol{E}(t) = \boldsymbol{e}_x E_x(t) + \boldsymbol{e}_y E_y(t)$, where $E_x(t) = E_0\sin(\omega t)$, $E_y(t) = E_1\cos(\omega t)$, $E_0 = E_\mathrm{L}/\sqrt{1+\epsilon^2}$, and $E_1 = \epsilon E_0$. Without loss of generality, we limit our discussions to the first laser half-cycle, where the offset angle is related to the time t_0 according to $\omega t_0 = \pi/2$. At this time, Eq. (3) says that $|\boldsymbol{p}| = p_y$, while the vector $\boldsymbol{r}_0$ (and therefore the Coulomb force $\boldsymbol{F}_\mathrm{c}$) acts along the x-axis. When the scattering angle θ' is small, we also have

$$\begin{aligned} p'_x &\approx |\Delta\boldsymbol{p}|, \quad p'_y \approx p_y, \\ \tan\left(\frac{\theta}{2}\right) &= \tan\left(\frac{\theta'}{2}\right) \approx \sin\left(\frac{\theta'}{2}\right) \approx Z/(p^2 r_0). \end{aligned} \tag{6}$$

A sketch of the scattering picture described by the CS-SFA model is presented in Fig. 1.

According to Eq. (6), the offset angle θ can be further written as

$$\theta \approx \arctan\left(\frac{2Z}{p^2 r_0}\right). \tag{7}$$

Here, $p = |\boldsymbol{p}| = p_y = v_y(t_0) - A_y(t_0)$. As the momentum p considers the nonzero exit velocity $v_y(t_0)$, we call the expression for θ nonadiabatic. Note that at the peak time t_0 of $E_x(t)$ relative to the offset angle, $|v_x(t_0)| = 0$. Accordingly, as in the TRCM model,[25] assuming that $\boldsymbol{v}_i - \boldsymbol{A}(t_0) \approx -\boldsymbol{A}(t_i)$, we can also define a lag time $\tau = t_i - t_0$. Considering that τ is a small quantity, at the peak time t_0, we also have $|\boldsymbol{A}(t_i) - \boldsymbol{A}(t_0)| \approx E_0\tau = |\boldsymbol{v}_i| = |\Delta\boldsymbol{p}|$. Then, according to Eq. (5), we also have

$$\tau \approx \frac{2Z}{E_0 p r_0} \tag{8}$$

with $p = p_y = v_y(t_0) - A_y(t_0)$. Considering that for hydrogen-like atoms, $Z \approx \sqrt{2I_\mathrm{p}}$, and assuming that $r_0 \approx I_\mathrm{p}/E_0$ (as in Ref. [23]), we also have

$$\theta \approx \arctan\left(\frac{2\sqrt{2}E_0}{p_y^2\sqrt{I_\mathrm{p}}}\right) \tag{9}$$

with $\tau \approx 2\sqrt{2}/(p_y\sqrt{I_\mathrm{p}})$. In the paper, we will perform nonadiabatic calculations using the above expression.

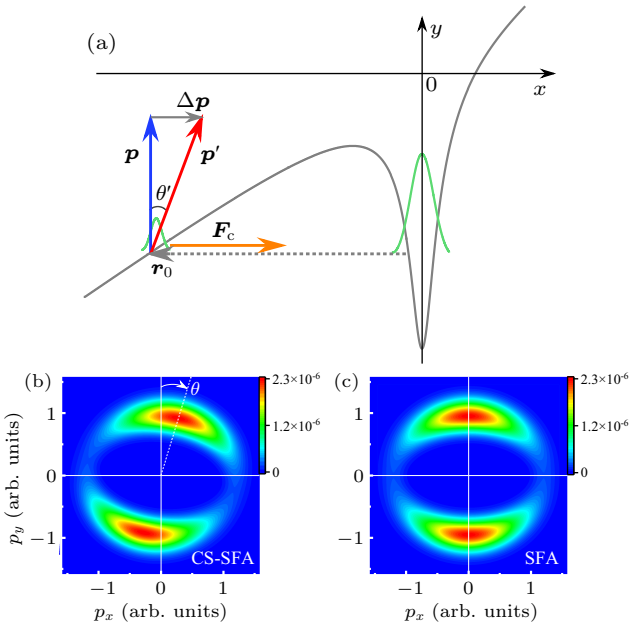


Fig. 1. A sketch of the Coulomb scattering picture described in CS-SFA. When the tunneling electron exits the barrier at the laser-field peak time t_0 at the position $\boldsymbol{r}_0$ with a momentum $\boldsymbol{p}$, it is scattered by the Coulomb force $\boldsymbol{F}_\mathrm{c}$, resulting in a momentum shift $\Delta\boldsymbol{p}$ and the final momentum $\boldsymbol{p}' = \boldsymbol{p} + \Delta\boldsymbol{p}$, as shown in (a). In (b) and (c), we plot the PMDs of the H atom obtained using the CS-SFA and SFA models, respectively. The PMD of CS-SFA in (b) shows a rotation characterized by the offset angle θ. The scattering angle θ' between $\boldsymbol{p}$ and $\boldsymbol{p}'$ in (a) amounts to the offset angle θ in (b). In contrast, the PMD of SFA in (c) does not show the rotation. The laser parameters used in the calculations are $I = 2\times10^{14}$ W/cm^2, $\lambda = 800$ nm, and $\epsilon = 0.84$.

2.2.3. Adiabatic approximation

By neglecting the term $v_y(t_0)$ in the expression of p_y, we can also obtain the adiabatic descriptions of θ and τ. By further considering $\tan\theta \approx \theta$ for a small angle θ and $p_y \approx -A_y(t_0) = \epsilon E_0/\omega$, we obtain

$$\theta \approx \frac{2\sqrt{2}\omega^2}{\epsilon^2 E_0\sqrt{I_\mathrm{p}}} \tag{10}$$

with $\tau \approx 2\sqrt{2}\omega/(\epsilon E_0\sqrt{I_\mathrm{p}})$. From Eq. (10), we also see $\theta \approx \omega\tau/\epsilon$. This is just the empirical relation between the angle θ and a time τ given in attoclock. Here, this relation is obtained from the adiabatic version of CS-SFA, which gives clear physical definitions of θ and τ, namely, the CS angle θ and the scattering time τ. In the paper, we perform the relevant adiabatic calculations using Eq. (10). It should be noted that the above adiabatic expression of Eq. (10), which does not

consider the initial velocity $v_y(t_0)$ at the tunnel exit, is similar to the expression of Eq. (5) in Ref. [23] for the KR model but differs by a constant factor of two. We will discuss this point in detail later.

2.2.4. PMDs

The momentum shift $\Delta\boldsymbol{p}$ induced by $\boldsymbol{F}_c$ is always contrary to the vector $\boldsymbol{r}_0$, as shown in Fig. 1(a). Then, by considering Eq. (5), we obtain $\Delta\boldsymbol{p} = -|\Delta\boldsymbol{p}|\boldsymbol{r}_0/r_0 = -2Z\boldsymbol{r}_0/(pr_0^2)$ and $\boldsymbol{p}' = \boldsymbol{p} + \Delta\boldsymbol{p}$. By assuming that the scattering influences only the saddle-point momentum $\boldsymbol{p} \equiv \boldsymbol{p}(t_0)$ of Eq. (3) at an arbitrary time t_0 and does not change the corresponding amplitude $c(\boldsymbol{p}) \approx \mathrm{e}^{-b}$,[2] we can obtain the CS-SFA amplitude $c(\boldsymbol{p}')$ directly from the SFA with $c(\boldsymbol{p}') \equiv c(\boldsymbol{p})$. Here, b is the imaginary part of the semiclassical action $S(\boldsymbol{p}, t_s)$. This CS-SFA therefore provides a simple approach for studying the Coulomb effect in the strong-field ionization of atoms. The CS-SFA prediction of the PMD for H is presented in Fig. 1(b).

3. Results and discussion

Next, we apply the CS-SFA to different atoms using diverse laser parameters and discuss the potential mechanism by comparing the CS-SFA to other theoretical models.

3.1. Applications to different targets

In Fig. 2, we first compare the predictions of the CS-SFA to experimental measurements for the offset angle of the He atom.[35] Due to the uncertainty in calibrating the laser intensity in experiments, the experimental results are presented for nonadiabatic and adiabatic calibration procedures, corresponding to Eqs. (9) and (10) in our treatments, respectively. First, for nonadiabatic cases, the predictions of Eq. (9) agree with the experimental results for higher laser intensities of $I > 1.2 \times 10^{14}$ W/cm^2. For lower laser intensities, the experimental angles increase very quickly as the intensity decreases, while the model angles change slowly. When the laser intensity is low, quantum effects beyond tunneling, such as multiphoton transitions, can play an important role in ionization. In this case, the current tunneling-based treatment may not give a full description of ionization. In adiabatic cases, the results of Eq. (10) generally agree with the experimental data. Since Eq. (10) is an approximation of Eq. (9) in the CS-SFA, in the following discussions of Figs. 3–5, we will focus on the results of Eq. (9). On the other hand, because the adiabatic expression of Eq. (10) is similar to the KR expression of Eq. (5) in Ref. [23], we can analyze the difference between the KR model and the CS-SFA by comparing the predictions of Eqs. (9) and (10). Relevant discussions are presented in Subsection 3.2.

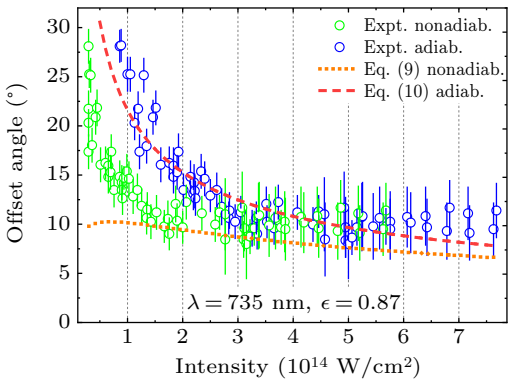


Fig. 2. Prediction of the offset angle in He using the CS-SFA at various laser intensities. Dots: experimental results for the nonadiabatic (green circle) and adiabatic (blue circle) laser-intensity calibrations in Ref. [35]. Lines: predictions of Eq. (9) for the nonadiabatic CS-SFA (orange dotted) and Eq. (10) for the adiabatic variant (red dashed). Laser parameters used are as shown.

In Fig. 3, we apply our model to the H atom, comparing or results to the experimental and 3D-TDSE results given in Ref. [15]. For lower laser intensities such as $I < 2 \times 10^{14}$ W/cm^2, the predictions of Eq. (9) are about one to two degrees (corresponding to about 7.5 attoseconds to 15 attoseconds in terms of time delay) larger than the experimental and TDSE results. The difference between them becomes somewhat larger at higher laser intensities. For high intensities, the ionization of H at $I_p = 0.5$ a.u. is strong, and therefore the ground-state depletion is also remarkable. This remarkable depletion effect is not considered in the present SFA-based scattering model. We note that in Ref. [15], the time delay τ is obtained from the angle θ using the relation $\theta \approx \omega\tau/\epsilon$. This relation holds in our theory in the adiabatic approximation. Here, for direct comparison with the results given in Ref. [15], we also use this relation to evaluate the delay τ from the angle θ of Eq. (9).

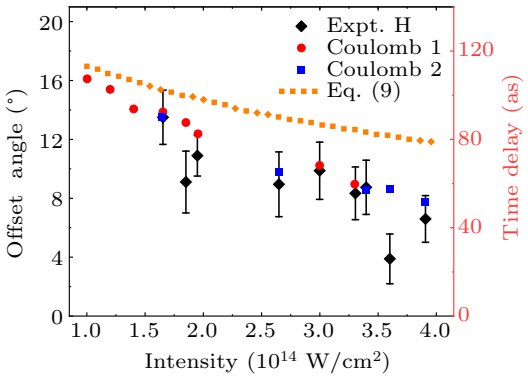


Fig. 3. Prediction of the offset angle and the time delay in H using the CS-SFA at diverse laser intensities. Dots: experimental (black diamond) and 3D-TDSE (red circle and blue square) results given in Ref. [15]. Orange line: predictions of Eq. (9) for the nonadiabatic CS-SFA. Laser parameters used are as shown. The time delay τ (right axis) is obtained from the offset angle θ with $\theta \approx \omega\tau/\epsilon$.

We further apply our model to additional targets such as He, Ar,[5] H_2[16] and H[18] at a wider range of laser parameters. Relevant results are presented in Fig. 4 and compared to actual and numerical experiments. Equation (9) gives a

good description of the experimental results for He and Ar shown in Figs. 4(a) and 4(b). It also gives a good explanation of the experimental results for the small molecule H_2 in Fig. 4(c). The predictions of Eq. (9) also agree with the TDSE results for H obtained in other numerical experiments from $I = 0.5 \times 10^{14}$ W/cm^2 to $I = 2.5 \times 10^{14}$ W/cm^2, as seen in Fig. 4(d). Here, for lower and higher laser intensities, the model results for H differ remarkably from the TDSE results, which is similar to the cases discussed for Figs. 2 and 3.

In Fig. 5, we further compare the predictions of the CS-SFA model to the experimental[36] and TDSE[26] results for the ellipticity dependence of the offset angle in attoclock. While the prediction of the model for the p_y component of the drift momentum related to the offset angle in attoclock agrees well with the experimental and TDSE results in Fig. 5(a), the model prediction for the p_x component differs remarkably from experimental and TDSE results for small ellipticity but agrees with those for large ellipticity in Fig. 5(b). The offset angle in Fig. 5(c) is similar to that for p_x shown in Fig. 5(b).

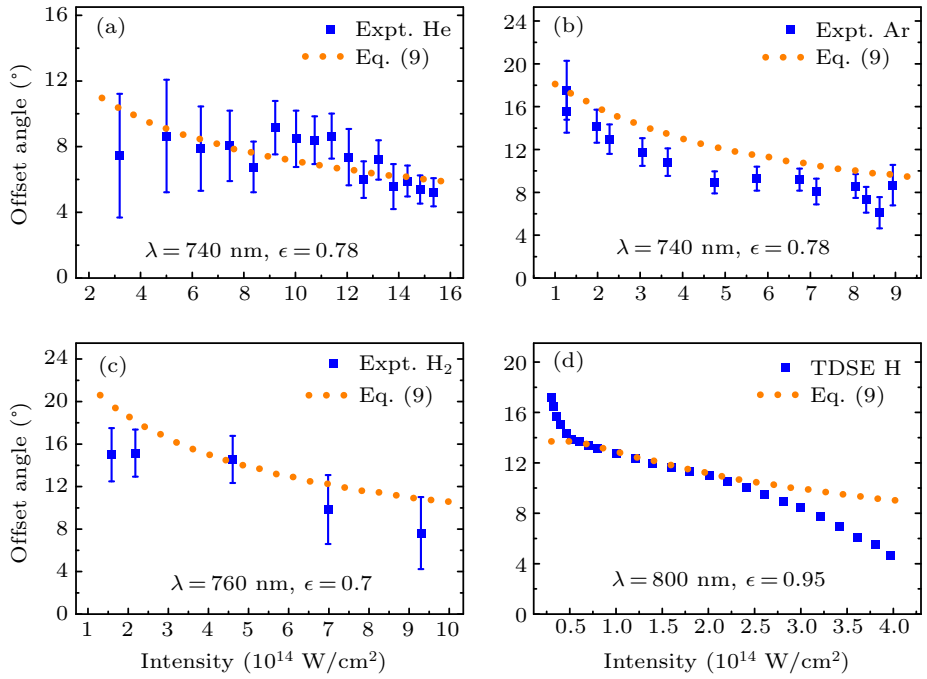


Fig. 4. Application of the CS-SFA model to further cases to predict the offset angle at diverse laser intensities. Blue square dots: experimental results for He (a) and Ar (b) from Ref. [5] and for H_2 (c) from Ref. [16], and 3D-TDSE results for H (d) from Ref. [18]. Orange lines: predictions of Eq. (9) for the nonadiabatic CS-SFA model. Laser parameters used are as shown.

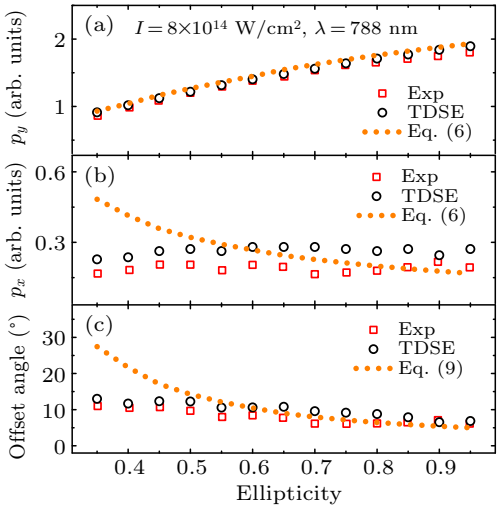


Fig. 5. Comparisons of the drift momenta (p_x, p_y) relative to the offset angle θ from experimental results,[36] the TDSE model,[26] and the CS-SFA model (Eq. (6)) with $Z \approx \sqrt{2I_p}$ and $r_0 \approx I_p/E_0$ at different laser ellipticities ϵ. In (c), the experimental offset angles are obtained using $\theta \approx \arctan(p_x/p_y)$ and the CS-SFA offset angles are obtained using Eq. (9). Laser parameters used are $I = 8 \times 10^{14}$ W/cm^2 and $\lambda = 788$ nm.

The results shown in Figs. 2–5 suggest that the CS-SFA model is more applicable to high ellipticity and moderate laser intensities. The potential reason for this will be discussed in detail below.

3.2. Analyses and comparisons

Comparisons to the KR model The original KR model[23] uses classical Coulomb scattering theory to describe the strong-field tunneling ionization of atoms. The KR model is comparable to experiments at lower laser intensities. As the laser-induced tunneling ionization of atoms includes both quantum and classical processes, we further introduce the SFA initial conditions related to the quantum properties of tunneling into the KR model and develop the semiclassical CS-SFA model that consists of simple formulas. The results in Figs. 2–5 show that the predictions of the CS-SFA model agree with attoclock experiments over a wider range of laser and atomic parameters. This agreement indicates that both system symmetry (as reflected in classical Coulomb scattering[23]) and quantum effects (as reflected in the initial conditions[22]) play

important roles in tunneling ionization.

The main differences between the predictions of the KR and CS-SFA models arise for the following reasons. First, the CS-SFA model considers the initial velocity $v(t_0)$ related to tunneling in the expression for the momentum $\boldsymbol{p}'$ (Eq. (4) in this paper), while the KR model neglects this velocity. For a specific atom, the value of this velocity is generally larger for larger Keldysh parameters, which correspond to lower laser intensities and higher laser frequencies. Second, when we ignore this velocity, an adiabatic expression for the offset angle in the CS-SFA model can be obtained (Eq. (10) in this paper), which is similar to the expression in the KR model but multiplied by two relative to the expression in the KR model (Eq. (5) in Ref. [23]). In other words, multiplying the KR prediction by a factor of two yields the adiabatic prediction made by the CS-SFA model. We take the results in Fig. 2 as an example to discuss the difference between the KR model and the CS-SFA model. From Fig. 2, one can observe that the adiabatic prediction made by the CS-SFA model agrees with the adiabatic experimental data, suggesting the applicability of the CS-SFA model. Next, let us neglect the absolute amount of the offset angle and focus on the laser-parameter dependence of the angle. This dependence is also known as the scaling law, which reflects the fundamental dynamical property of the laser-driven system in tunneling ionization. In this sense, we can directly understand the adiabatic prediction of the CS-SFA model as the KR prediction. Since, at low laser intensities, the value of $|A_y(t_0)| = E_1/\omega$ is small for the peak time t_0 of the laser field, the velocity $v_y(t_0)$ has a larger influence on the momentum $p_y = v_y(t_0) - A_y(t_0)$ and therefore on the offset angle $\theta \approx p_x/p_y$. As a result, the predictions of the adiabatic and nonadiabatic CS-SFA models for the laser intensity dependence of the offset angle differ remarkably from each other in cases of low intensity, and this difference decreases with increasing laser intensity, as shown in Fig. 2.

Comparisons to other models Next, we compare the CS-SFA model to other Coulomb-inclusive strong-field models. In contrast to the TC-SFA model,[22] the ARM theory,[18] and the extended KR model,[23] the CS-SFA model describes the Coulomb effect using classical Coulomb scattering theory. Rather than relying on numerical[22] solutions of the Newton equation that include both the electric and Coulomb forces, analytical solutions of the same equation,[23] or numerical solutions[18] of the saddle-point equation including the Coulomb force, the CS-SFA adopts a classical approach to model the Coulomb interaction. The KR is able to give analytical and concise expressions composed of basic laser and atomic parameters, such as laser intensity, laser frequency, laser ellipticity, and ionization potential, for observable values such as the offset angle in attoclock. In comparison with the KR approach,[25] both the CS-SFA and TRCM models consider the Coulomb effect with an emphasis on the central symmetry of the atomic Coulomb potential. The TRCM assumes that at the tunnel exit, the tunneling electron is still held in a quasi-bound state. This state approximately agrees with the virial theorem,[28] through which the Coulomb-related velocity $\boldsymbol{v}_i$ can be evaluated. The CS-SFA model assumes Coulomb-induced classical elastic scattering after tunneling, and the Coulomb-related velocity $\boldsymbol{v}_i$ can be calculated through the classical Coulomb scattering formula. Given the above differences in describing the velocity $\boldsymbol{v}_i$, the scaling laws for the dependence of the offset angle θ on laser amplitude $E_{\rm L}$, ellipticity ϵ, and ionization potential $I_{\rm p}$ are different in the TRCM and CS-SFA models. The scaling law is $\theta \sim \epsilon^{-2}{E_0}^{-1}{I_{\rm p}}^{-1/2} \sim (1+\epsilon^2)^{1/2}\epsilon^{-2}{E_{\rm L}}^{-1}{I_{\rm p}}^{-1/2}$ in the CS-SFA model (see Eq. (10) in this paper), while it is $\theta \sim \epsilon^{-1}{E_0}^{-1/2}{I_{\rm p}}^{-1/4} \sim (1+\epsilon^2)^{1/4}\epsilon^{-1}{E_{\rm L}}^{-1/2}{I_{\rm p}}^{-1/4}$ in the TRCM model (see Eq. (12) in Ref. [26]). Comparing the predictions of the CS-SFA model in this paper and those of the TRCM model in Refs. [25–27], one can observe that although the predictions of the TRCM and CS-SFA models are comparable for some cases discussed here, the scaling law given by the TRCM model agrees better with the experimental results. However, the CS-SFA model provides a simpler and more intuitive physical picture of the origin of the offset angle.

SAE approximation We have also used the single-active-electron (SAE) approximation when simulating the strong-field tunneling ionization of atoms and molecules using the CS-SFA model proposed in this paper. The SAE approximation assumes that only one valence electron is active in the system and considers the other electrons and atomic nucleus as a whole. This approximation has been widely used in strong-field physics to simplify the problem studied, such as in Refs. [16,17,21,22], etc. In this approximation, multielectron atoms such as He and Ar can be treated as hydrogen-like ions with only one electron and one 'nucleus', so we can obtain analytical expressions for the observable values in our model, such as the offset angle in attoclock. With this approximation, our simulations based on CS-SFA show that the results obtained can be quantitatively compared with relevant experimental data (as shown in Figs. 2–5 of this paper). These results support the use of the SAE approximation. However, this applicability is also influenced by the laser parameters. We will discuss this point in detail below.

Applicability of the CS-SFA model In the following, we discuss the scope of application of the CS-SFA model. The CS-SFA model introduces the initial conditions given by the SFA into the original KR model. Therefore, the applicability of this model is closely related to the applicability of the SFA. It is well known that the SFA is more applicable when the Keldysh parameter[31] γ is smaller than unity, i.e., $\gamma = \omega\sqrt{2I_{\rm p}(1+\epsilon^2)}/E_{\rm L} < 1$. Therefore, this condition also

holds for the CS-SFA model. Specifically, the CS-SFA model is more applicable at intermediate laser intensities. For high laser intensities, the ionization is strong, and over-barrier ionization beyond tunneling can occur. This over-barrier effect is not considered in our current model. In multielectron systems, in addition to the active electron, other electrons may also be excited and ionized at high laser intensities. In this case, the potential function of the system is more complex than that of a hydrogen-like ion, and the SAE approximation is inapplicable. This may lead to deviations between CS-SFA model predictions and experimental data at high laser intensities, such as the deviation shown in Fig. 2. For low laser intensities, the ionization is weak, which means that fewer photoelectrons can be collected, and noise related to some unexpected effects can influence the PMD and therefore affect the resolution of the offset angle. In addition, the CS-SFA model works well at relatively longer laser wavelengths. For very short laser wavelengths, single-photon or several-photon transitions dominate in ionization, and inner-shell electrons can also be excited in multielectron systems. These effects have not been fully considered in the SFA model on which the CS-SFA model is based. Besides, the CS-SFA model works better for intermediate and high laser ellipticities. For small ellipticities, interference between long and short electron trajectories can affect the resolution of the offset angle in PMD. Therefore, the CS-SFA model, along with the SAE approximation, can provide better attoclock predictions in cases of relatively large ellipticity, longer laser wavelengths, and intermediate laser intensities with moderate ionization yields. It is worth noting that using the classical CS formula to describe the Coulomb effect in atomic strong-field ionization is only an approximate method that emphasizes the central symmetry of the system. Therefore, even for applicable laser and atomic parameters, the predictions of the CS-SFA model may differ somewhat from experimental results.

4. Conclusion

In conclusion, we have studied the ionization of atoms in strong elliptically polarized laser fields with high ellipticity. Based on the quantum model of the SFA and the classical model of KR Coulomb scattering, we have developed a semiclassical model, called the CS-SFA model, to describe the ionization process. The latter can be understood as a two-step process of tunneling and classical motion. The CS-SFA model describes the tunneling of the electron under the barrier through the SFA combined with saddle-point theory characterized by imaginary time. It describes the classical motion of the electron after tunneling using the KR model, which is characterized by the Coulomb scattering induced by the central symmetric Coulomb potential. These two steps are connected at the tunnel exit, which can also be understood as the boundary between quantum and classical motion. The exit velocity and exit position given by the SFA at the tunneling-out time are used as the initial conditions for the classical Coulomb scattering process. We focus on the offset angle in PMD, which has been widely used in attoclock experiments as the characteristic observable. Simple expressions for the offset angle are derived in the CS-SFA model, which show that this angle corresponds to the classical scattering angle but is remarkably influenced by the initial conditions given by the SFA at the tunnel exit. The predictions of the CS-SFA model agree with recent attoclock experiments over a wide range of laser and atomic parameters, suggesting the applicability of the model. We also compared the CS-SFA model to other Coulomb-included strong-field models and discussed the potential differences. Our results show that both system symmetry and quantum effects play important roles in tunneling ionization. This suggests that system symmetry can significantly simplify the theoretical description of the Coulomb effect in strong-field ionization, allowing for the construction of analytical strong-field models. These results may help researchers understand and study experimental phenomena in attosecond-resolved measurements.

Acknowledgements

Project supported by the National Natural Science Foundation of China (Grant Nos. 12174239, 12347165, and 12404330), Shaanxi Fundamental Science Research Project for Mathematics and Physics (Grant No. 23JSY022), Natural Science Basic Research Program of Shaanxi (Grant No. 2022JM-015), Hebei Natural Science Foundation (Grant No. A2022205002), and Science and Technology Project of Hebei Education Department (Grant No. QN2022143).

References

[1] Becker W, Grasbon F, Kopold R, Milošević D B, Paulus G G and Walther H 2002 *Adv. At. Mol. Opt. Phys.* **48** 35
[2] Lewenstein M, Kulander K C, Schafer K J and Bucksbaum P H 1995 *Phys. Rev. A* **51** 1495
[3] Eckle P, Smolarski M, Schlup P, Biegert J, Staudte A, Schöffler M, Muller H G, Dörner R and Keller U2008 *Nat. Phys.* **4** 565
[4] Eckle P, Pfeiffer A N, Cirelli C, Staudte A, Dörner R, Muller H G, Büttiker M and Keller U 2008 *Science* **322** 1525
[5] Pfeiffer A N, Cirelli C, Smolarski M, Dimitrovski D, Abu-samha M, Madsen L B and Keller U 2012 *Nat. Phys.* **8** 76
[6] Pfeiffer A N, Cirelli C, Smolarski M and Keller U 2013 *Chem. Phys.* **414** 84
[7] Shvetsov-Shilovski N I, Lein M, Madsen L B, Räsänen E, Lemell C, Burgdörfer J, Arbó D G and Tőkési K 2016 *Phys. Rev. A* **94** 013415
[8] Trabert D, Anders N, Brennecke S, Schöffler M S, Jahnke T, Schmidt L Ph H, Kunitski M, Lein M, Dörner R and Eckart S 2021 *Phys. Rev. Lett.* **127** 273201
[9] Douguet N and Bartschat K 2022 *Phys. Rev. A* **106** 053112
[10] Dou Y K, Fang Y Q, Ge P P and Liu Y Q 2023 *Chin. Phys. Lett.* **40** 033201
[11] Cao D D, Pan X F, Zhang J and Liu X S 2023 *Chin. Phys. B* **32** 034204
[12] Landsman A S, Weger M, Maurer J, Boge R, Ludwig A, Heuser S, Cirelli C, Gallmann L and Keller U 2014 *Optica* **1** 343

[13] Camus N, Yakaboylu E, Fechner L, Klaiber M, Laux M, Mi Y H, Hatsagortsyan K Z, Pfeifer T, Keitel C H and Moshammer R 2017 *Phys. Rev. Lett.* **119** 023201

[14] Teeny N, Yakaboylu E, Bauke H and Keitel C H 2016 *Phys. Rev. Lett.* **116** 063003

[15] Sainadh U S, Xu H, Wang X, Atia-Tul-Noor A, Wallace W C, Douguet N, Bray A, Ivanov I, Bartschat K, Kheifets A, Sang R T and Litvinyuk I V 2019 *Nature* **568** 75

[16] Quan W, Serov V V, Wei M Z, Zhao M, Zhou Y, Wang Y L, Lai X Y, Kheifets A S and Liu X J 2019 *Phys. Rev. Lett.* **123** 223204

[17] Klaiber M, Hatsagortsyan K Z and Keitel C H 2015 *Phys. Rev. Lett.* **114** 083001

[18] Torlina L, Morales F, Kaushal J, Ivanov I, Kheifets A, Zielinski A, Scrinzi A, Muller H G, Sukiasyan S, Ivanov M and Smirnova O 2015 *Nat. Phys.* **11** 503

[19] Ma Y Z, Ni H C and Wu J 2024 *Chin. Phys. B* **33** 013201

[20] Brabec T, Ivanov M Yu and Corkum P B 1996 *Phys. Rev. A* **54** R2551

[21] Goreslavski S P, Paulus G G, Popruzhenko S V and Shvetsov-Shilovski N I 2004 *Phys. Rev. Lett.* **93** 233002

[22] Yan T M, Popruzhenko S V, Vrakking M J J and Bauer D 2010 *Phys. Rev. Lett.* **105** 253002

[23] Bray A W, Eckart S and Kheifets A S 2018 *Phys. Rev. Lett.* **121** 123201

[24] Serov V V and Kheifets A S 2022 *Phys. Rev. A* **105** 063106

[25] Chen C, Che J Y, Li W Y, Wang S, Xie X J, Huang J Y, Peng Y G, Xin G G and Chen Y J 2021 arXiv:2111.08491

[26] Che J Y, Huang J Y, Zhang F B, Chen C, Xin G G and Chen Y J 2023 *Phys. Rev. A* **107** 043109

[27] Che J Y, Chen C, Li W Y, Li W and Chen Y J 2023 *Acta Phys. Sin.* **72** 193301 (in Chinese)

[28] Chen Z Y, Shen S Q, Li Y P, Yang Z Q, Che J Y and Chen Y J 2025 to appear in *Phys. Rev. A*

[29] Xie X J, Chen C, Xin G G, Liu J and Chen Y J 2020 *Opt. Express* **28** 33228

[30] Che J Y, Chen C, Wang S, Xin G G and Chen Y J 2023 *New J. Phys.* **25** 013016

[31] Keldysh L V 1965 *Sov. Phys. JETP* **20** 1307

[32] Faisal F H M 1973 *J. Phys. B: At. Mol. Phys.* **6** L89

[33] Reiss H R 1980 *Phys. Rev. A* **22** 1786

[34] Landau L and Lifshitz E 1982 *Mechanics*, in Theorecial Physics Vol. 1 (Oxford: Elsevier)

[35] Boge R, Cirelli C, Landsman A S, Heuser S, Ludwig A, Maurer J, Weger M, Gallmann L and Keller U 2013 *Phys. Rev. Lett.* **111** 103003

[36] Landsman A S, Hofmann C, Pfeiffer A N, Cirelli C and Keller U 2013 *Phys. Rev. Lett.* **111** 263001